Available online at www.sciencedirect.com
ScienceDirect
Advances in Engineering Software 38 (2007) 698–709
ADVANCES IN ENGINEERING SOFTWARE
www.elsevier.com/locate/advengsoft

MicroARTMAP for pattern recognition problems

S. Rajasekaran [a,*], Vasantha Kalyani David [b]

[a] Department of Civil Engineering, PSG College of Technology, Coimbatore 641 004, Tamil Nadu, India
[b] Department of Computer Science, Avinashilingam Deemed University, Coimbatore, Tamil Nadu, India

Received 26 May 2006; received in revised form 14 October 2006; accepted 19 October 2006
Available online 8 December 2006

Abstract

Pattern recognition is an important aspect of a dominant technology such as machine intelligence. Domain specific fuzzy-neuro models particularly for the 'black box' implementation of pattern recognition applications have recently been investigated. In this paper, Sanchez's MicroARTMAP has been discussed as a pattern recognizer/classifier for the image processing problems. The model inherently recognizes only noise free patterns and in case of noise perturbations (rotations/scaling/translation) misclassifies the images. To tackle this problem, a conventional Hu's moment based rotation/scaling/translation invariant feature extractor has been employed. The potential of this model has been demonstrated on two problems, namely, recognition of alphabets and words and prediction of load from yield pattern of elasto-plastic analysis. The second example concerns with color images dealing with colored patterns. MicroARTMAP is also applied to other two civil engineering problems, namely (a) Indian Standard (IS) classification of soil and (b) prediction of earthquake parameters from the response spectrum in which no feature extractor step is necessary.

Keywords: MicroARTMAP; Soil classification; ART models; Neural networks; Earthquake; Yield pattern; Fuzzy ARTMAP; Indian Standard; Prandtl–Reuss

1. Introduction

The success that concerns the description or classification (recognition) of measurements is often an important component of intelligent systems. Diagnostic analysis of crack pattern by Chao and Cheng [1], structural damage assessment by Ishizuka et al. [2] and Watada et al. [3] and examination of soil cracking pattern are some of the problems on which pattern recognition (PR) techniques have been applied.

In the past, neural network (NN) and fuzzy logic (FL) have individually presented themselves as potential candidates for several approaches well suited for pattern classification applications. Kosko's fuzzy associative memory [4] has been used to present fuzzy association. Yamakawa and Tomoda [5] proposed a simple fuzzy neuron model for application in character recognition but failed to describe a specific learning algorithm. The aim of this paper is to build a pattern recognizer based on a fuzzy-neuro model that exhibits the following characteristics.

1. A less complex but powerful fuzzy neuro architecture.
2. Significant reduction in training.
3. Recognition of both monochrome and color images.
4. Tolerance to pattern perturbations (rotation, scaling and translation).

The adaptive resonance theory (ART) model by Moore [6] is one of the triumphs of modern neural network theory. The model combines the concepts of feedback stability between two layers of competing neurons with learning convergence of the synaptic pathways that connect the two layers. The synapses learn only if the two fields resonate in a dynamic equilibrium. The Fuzzy ART models of Carpenter and Gjaja [7] and Carpenter et al. [8] approximate surfaces in a fuzzy cube of high dimension [4]. Each pattern is a discrete fuzzy set. The ART system uses the

* Corresponding author. Tel.: +91 422 2594 430; fax: +91 422 2573 833.
E-mail address: drrajasekaran@gmail.com (S. Rajasekaran).

0965-9978/$ - see front matter © 2006 Elsevier Ltd. All rights reserved.
doi:10.1016/j.advengsoft.2006.10.008

degree of subset hood to control how well fuzzy patterns match. The system covers the decision surface with hyper-boxes as much as a feed forward fuzzy system covering a function's graph with rule patches. As the diversion of the space grows, there is rule explosion. The fuzzy ART model uses subset hood to control the fineness of the hyper box cover in a fixed fuzzy cube. The result blends the core concepts of fuzzy cubes and feed back neural networks in a novel and powerful architecture.

Kasuba's simplified fuzzy ARTMAP (SFAM) [9] was chosen to function as the core architecture. When compared to its predecessor, Carpenter's fuzzy ARTMAP, SFAM has reduced computational overhead and architectural redundancy. The MicroARTMAP is a modification of the Fuzzy ARTMAP that includes an inter-ART reset mechanism. This reset mechanism does not cause category proliferation and allows the correct treatment of exceptions. Category proliferation has been handled in Fuzzy ARTMAP by modifying the architecture or the training algorithm by MicroARTMAP as explained by Sanchez [10].

In order to overcome the problem of tolerance to pattern perturbation, features are extracted to be fed into MicroARTMAP as "pre-processed" inputs. Already Rajasekaran and Vijayalakshmi Pai [11,12] have used SFAM and Rajasekaran and Amalraj [13] ART1 architecture for image recognition.

This paper discusses MicroARTMAP, a neuro-fuzzy pattern recognizer. First, the MicroARTMAP and their learning equations are presented in brief. Next, the conventional Hu's moment invariants for the successful feature extraction are discussed. Finally, the structure of the pattern recognizer and the architecture for two problems, namely (a) recognition of letters and words and (b) prediction of load from the yield line pattern of elasto-plastic analysis of clamped plate which requires features are to be presented. The MicroARTMAP is also applied to two other civil engineering problems, namely (a) soil classification and (b) the prediction of earthquake parameters from response spectra.

2. Fuzzy art algorithm

The fuzzy ART system has three fields of nodes, namely F_0, F_1 and F_2. A field F_0 of nodes represents a current input vector and field F_1 receives both the bottom–up input from F_0 and top–down input from a field F_2 that represents the active code or category. The vector $\mathbf{I} = (I_1, \ldots, I_m)$ denotes F_0 activity in the interval $[0, 1]$ for $i = 1, 2, \ldots, M$. So $\mathbf{I}$ is a point in a fuzzy n-cube. $\mathbf{I} \in [0, 1]^n$. $\mathbf{x} = (x_1, x_2, \ldots, x_M)$ denotes F_1 activity and $y = (y_1, \ldots, y_N)$ denotes F_2 activity. The fuzzy **ART** notation is given in Fig. 1.

2.1. Weight vector

Associated with each F_2 category node is a vector $w_j = (w_{j1}, w_{j2}, \ldots, w_{jM})$ of adaptive weights. At first, all the

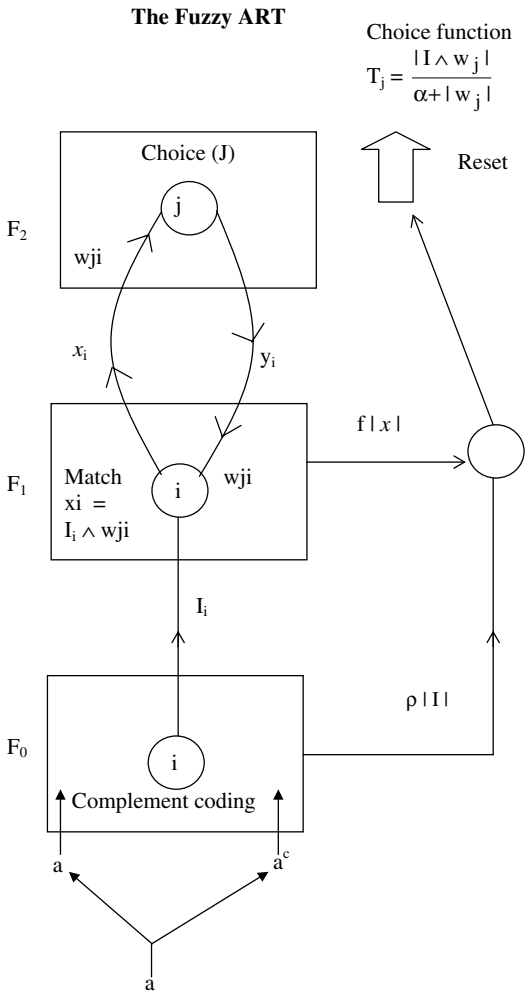

Fig. 1. Fuzzy ART notation.

weights $(w_{j1}(0) = \cdots = w_{jM}(0) = 1)$ are initialized to 1. Then each category is uncommitted. After a category codes its first input it becomes committed. w_j subsumes both the bottom–up and top–down weight vectors of ART1.

2.2. Parameters

A choice parameter $\alpha > 0$, a learning rate $\beta \in [0, 1]$ and a vigilance parameters $\rho \in [0, 1]$ fix the fuzzy art dynamics [14].

2.3. Category choice

Neural networks are in general very sensitive to absolute magnitude and fluctuations in inputs and may tend to swamp the performance of the network while predicting the desired outputs. Hence, the need for normalization of inputs so that the inputs correspond to the same range of values. Complement coding is applied as a normalization rule for preserving amplitude information. Thus, it represents the on-response and the off-response to an input vector. It also represents the presence of a particular feature in

the input pattern and its absence. For each input I and F_2 node j, the choice function T_j has the form

$$T_j(I) = \frac{|I \wedge w_j|}{\alpha + |w_j|} \tag{1}$$

where $\wedge$ is the fuzzy intersection given by

$(p \wedge q)_i \equiv \min(p, q)$ and the norm $|\cdot|$ is the fuzzy count $c(p)$ given by

$$|p| = \sum_{1=1}^{M} |p_i| \tag{2}$$

The index J denotes the chosen category.

$$T_J = \max\{T_j : j = 1, \ldots, N\}$$

If more than one T_j is maximal then the system chooses the category with the smallest j index. Thus, nodes become committed in order $j = 1, 2, 3, \ldots$. When the system chooses the Jth category then $y_J = 1$ and $y_j = 0$ for $y_j \neq J$. In a choice system the F_1 activity vector x obeys the equation

$$x = I \quad \text{if } F_2 \text{ is inactive} \tag{3}$$

$$I \wedge w_J \quad \text{if } J\text{th } F_2 \text{ node is chosen} \tag{4}$$

2.4. Resonance

Resonance occurs when

$$\frac{|I \wedge w_j|}{|I|} \geqslant \rho \tag{5}$$

where ρ is the vigilance criterion implying that when the Jth category becomes active, the resonance occurs if

$$|x| = |I \wedge w_j| \geqslant \rho |I| \tag{6}$$

Mismatch reset occurs when

$$\frac{|I \wedge w_j|}{|I|} < \rho \tag{7}$$

and thus if $|x| = |I \wedge w_j| < \rho |I|$ (8)

2.5. Learning

The weight vector w_j learns according to

$$w_j^{(\text{new})} = \beta(I \wedge w_j^{(\text{old})}) + (1 - \beta) w_j^{(\text{old})} \tag{9}$$

Fast learning corresponds to setting $\beta = 1$.

2.6. Fast-commit and slow-recode

For efficient coding of noisy input sets, it helps to set $\beta = 1$ when j is an uncommitted node. Then $\beta < 1$ is considered after the system already commits the category. The just-commit and slow recode by Moore [6] option makes $w_j^{(\text{new})} = i$, the first time category j becomes active. Complement coding solves the problem of many random inputs eroding the norm of weight vectors.

2.7. Normalization by complement coding

Normalization of fuzzy ART inputs prevents category proliferation. This normalization is done using complement coding as shown below.

The system normalizes the $F_0 \to F_1$ inputs if for some $\gamma > 0$

$$\sum_i I_i = |I| = \gamma \tag{10}$$

for all inputs.

If $a \in [0, 1]^M$ denotes original input, then

$$I = (a, a^c) \in [0, 1]^{2M} \tag{11}$$

where

$$a^c = \{a_i^c\} \quad \text{and } a_i^c = 1 - a_i \tag{12}$$

The new F_0 layer input vector I is complement coded and both I and w_j are of dimensions $2M$:

$$I = (a, a^c) = (a_1, a_2, \ldots, a_M, a_1^c, \ldots, a_M^c) \tag{13}$$

So I is a point in the double-sized fuzzy cube $[0, 1]^{2M}$.

One way to normalize a vector 'a' is to divide by the fit count

$$I = \frac{\bar{a}}{|a|} \tag{14}$$

Compliment coding represents both on-response and the off-response to an input vector $\bar{a}$. In the simplest form $\bar{a}$ represents on-response and $\bar{a}^c$ represents off-response. I has the same fuzzy or entropy structure as does its terms $\bar{a}$ and $\bar{a}^c$.

The system automatically normalizes a complement coded input because

$$I = |(\bar{a}, \bar{a}^c)| \tag{15a}$$

$$= \sum_{i=1}^{M} ai + \Sigma\left(M - \sum_{i=1}^{M} ai\right) \tag{15b}$$

$$= M \tag{15c}$$

with complement coding the initial condition

$$w_{j1}(0) = w_{j2}(0) \cdots = w_{j2M}(0) = 1 \tag{16}$$

Both I and w_j are of dimension $2M$.

2.8. MicroARTMAP algorithm (supervised neural network architecture) [10]

The architecture of MicroARTMAP is the same as fuzzy ARTMAP. MicroARTMAP uses two fuzzy ART modules ART^a and ART^b that link together via an inter-ART module F^{ab} called a map field. The map field forms predictive association between categories and realizes the ARTMAP match tracking rule. Match tracking increases ART^a vigilance parameter ρ^a in response to a predictive error or mismatch at ART^b. Match tracking reorganizes category structure so that subsequent presentations of the input do

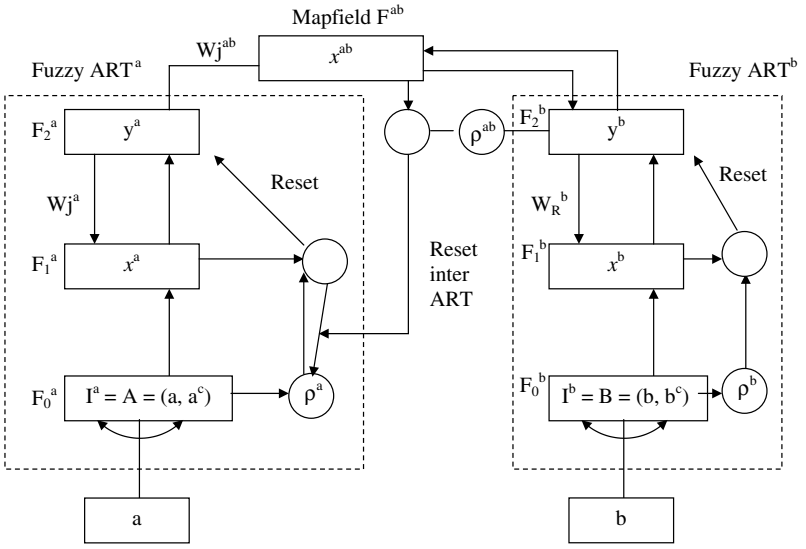

Fig. 2. MicroARTMAP architecture.

not repeat the error. The MicroARTMAP architecture is shown in Fig. 2. The learning is similar to FUZZY ARTMAP and herein we give the details of MicroARTMAP as given by Sanchez et al. and the reader is advised to refer to the paper [10].

3. Training of MicroARTMAP

All the weights are initialized to 1 as all categories are uncommitted:

$$w_{jk}^{ab} = 0, \quad j = 1, \ldots, N^a \quad k = 1, \ldots, N^b \tag{17}$$

The starting vigilance is set to 0 to minimize the number of categories.

Present the input–output pairs (a, b).

When a pattern 'a' is presented to **ART**^{a}, a category J is selected according to the choice function:

$$T_j = \frac{|I \wedge w_j|}{\alpha + |w_j|} \tag{18}$$

If it is a newly committed category then $\rho_J = \rho^a$.

The reset condition is evaluated as $\rho_J = \frac{|I \wedge w_j|}{|I|} \geqslant \rho$ where $\rho \in [0, 1]$, i.e. J node is active.

If this condition is not satisfied, this node will be inhibited and new search triggered.

Pattern b is presented to ART^b selecting the Kth category

Map field activity is given by

$$x^{ab} = \begin{cases} y^b + w_j^{ab} & \text{if } j\text{th } F_2^b \text{ node is active} \\ w_j^{ab} & \text{if } j\text{th } F_2^a \text{ node is active } F_2^b \text{ is inactive} \\ y^b & \text{if } F_2^a \text{ is inactive } F_2^b \text{ is active} \\ 0 & \text{if } F_2^a \text{ is inactive } yf_2^b \text{ is inactive} \end{cases} \tag{19}$$

3.1. Inter art reset

After x^{ab} the map field activity has been calculated, replacing p_j and p_{jk} by

$$p_{jk} = \frac{x_k^{ab}}{|x^{ab}|} \quad \text{if } j = J$$

$$p_j = \frac{x^{ab}}{|x^{ab}| + \sum_{i=1, i\neq j}^{N^a} |w_i^{ab}|} \tag{20}$$

$$p_{jk} = \frac{|w_{jk}^{ab}|}{|w_j^{ab}|} \quad \text{otherwise}$$

$$p_j = \frac{w_j^{ab}}{|x^{ab}| + \sum_{i=1, i\neq j}^{N^a} |w_i^{ab}|} \tag{21}$$

The contribution to the total entropy of the Jth unit if allowed to learn this pattern, h_j is calculated.

If $h_J > h_{max}$, then the category is too entropic and the Jth node in ART^a is inhibited by setting $T_J(I^a) = 0$, for the rest of this pattern presentation. Its vigilance parameter is not valid. Other categories will be chosen in ART^a until the entropy contribution criterion is met. When previously uncommitted category is selected say J^i then

$$P_{J_k^i} = 1 \quad \text{while } p_{jk} = 0 \text{ for } k \neq K \tag{22}$$

and $h_J = 0$. Then the weights in ART^a and ART^b are updated and also in the map field by $w_j^{ab} = x^{ab}$.

3.2. Offline evaluation

The off-line map field is initialized by $V_{J_k^{ab}} = 0$, $j = 1, \ldots, N^a$, $k = 1, \ldots, N^b$ after all patterns have been processed and the data are presented again to update these weights. A test on the training data is done and results are stored in weights. The entropy H is computed and compared to H_{max}.

If $H > H_{\max}$, then mapping defined by MICRO ART MAP is too entropic.

The ART^{a} has a node J that has maximal contribution to the total entropy.

$J = \arg\max\ h_j,\ j = 1, \ldots, N^{a}$ is searched and removed (i.e. $w_j^{a} = 1,\ w_j^{ab} = 0$).

The baseline vigilance is set to

$$p^{a} = \frac{|W_j|}{M^{a}} = 1 - \frac{R_j}{M^{a}} + \Delta\rho \tag{23}$$

This is done so that $R_J \leqslant M(1 - p^{a})$ (the category size is bounded).

All the patterns that previously selected the Jth ART^{a} category are presented and the rest are not presented. This process continues till

$H < H_{\max}$.

3.3. MicroARTMAP prediction

The Jth ART^{a} node is selected so that $T_J(I)$ value is highest and then the node corresponding to the K_J^{th} ART^{b} category is predicted:

$$K_J = \arg\max_h\{W_{jk}^{ab},\ k = 1, \ldots, N^{b}\}. \tag{24}$$

where K_J has the most frequent association to node J.

3.4. Fast learning in MicroARTMAP

When $\rho^{a} = 0$, $h_{\max} = 0$, fast learning is assumed. All patterns associated with a given class label will be inside the same ART^{a} hyper box which is arbitrarily large. The off-line evaluation will measure the probabilistic overlapping of the created hyper boxes. This is related to the number of patterns that select a different category when inter-ART reset is enabled and when it is disabled. This happens as the inter-ART reset does not raise ART^{a} vigilance. Overlapping of patterns will be large if $H > H_{\max}$. Learning is stopped when $H = 0$ that is when there is no overlapping in the input space. The hyper box to be refined is deleted and all patterns that previously selected that particular hyper box are presented again. Smaller hyper boxes are forced to cover the same region. Through this batch learning process, large hyper boxes are placed in regions where all patterns have the same class label, while small hyper boxes are placed in the boundaries between classes. Populated exceptions are handled with one large hyper box which is a general rule and a specific rule is represented by one smaller hyper box.

4. MicroARTMAP rules

The MicroARTMAP rules are extracted from the weights in the form.

4.1. IF a is c_j THEN output is L_K (priority p_i)

This means that pattern 'a' selects the jth category and L_K is the predicted label. The most general rule, i.e. the category with largest hyper box is evaluated. If the first rule is impure, then MicroARTMAP dynamically finds some category that arguments the mutual information between input and output partitions. When entropy has been reduced sufficiently MicroARTMAP training algorithms stops.

5. Feature extractor – moment based invariants [11,12]

Moments are extracted features that are derived from raw measurements. In practical imagery, images are subjected to various geometric disturbances or pattern perturbations. It is therefore necessary that features that are invariants to orientations be used for purposes of recognition or classification. For 2D images moments have been used to achieve Rotation (R), Dilation (D) and Translation (T) invariants.

The normalized moments η is defined as

$$\eta_{pq} = \mu_{pq}/\mu_{00}^{((p+q)/2+1)} \tag{25}$$

where $(p + q) = 2, 3 \ldots$ From Eq. (25), constraining $(p, q \leqslant 3)$ and using the tools of invariant algebra, a set of seven **RST** invariant features using Hu's moment invariants (but calculated with respect to centre of rotation) as shown in Table 1 may be derived. Those images, which are similar, are classified as belonging to the same class. In other words, images that are perturbed (rotated, scaled or translated) versions of the given nominal pattern are all classified as belonging to a class.

Visual image data can be either binary (for monochrome images) or real (for color images). In Hu's moment features formulae, $f(x, y) = 0$ or 1 based on whether the pixel is dark or bright. On the other hand, the intensity is represented by various shades with $0 \leqslant f(x, y) \leqslant 1$, indicating that the density lies anywhere between the ends of a spectrum; very dark to very bright thus representing color images. However, the image function $f(x, y)$ is constant over any pixel region.

Table 1
Normalized Hu's moments

$\phi_1 = \eta_{20} + \eta_{02}$
$\phi_2 = (\eta_{20} - \eta_{02})^2 + 4\eta_{11}^2$
$\phi_3 = (\eta_{30} - 3\eta_{12})^2 + (3\eta_{21} + \eta^{03})^2$
$\phi_4 = (\eta_{30} + \eta_{12})^2 + (\eta_{21} + \eta_{03})^2$
$\phi_5 = (\eta_{30} - 3\eta_{12})(\eta_{30} + \eta_{12})\lfloor(\eta_{30} + \eta_{12})^2 - 3(\eta_{21} + \eta_{03})^2\rfloor + 3(\eta_{21} - \eta_{03})(\eta_{21} + \eta_{03}) + \lfloor(3\eta_{30} + \eta_{12})^2 - 3(\eta_{21} + \eta_{03})^2\rfloor$
$\phi_6 = (\eta_{20} - \eta_{02})\lfloor(\eta_{30} + \eta_{12})^2 - 3(\eta_{21} + \eta_{03})^2\rfloor + 4\eta_{11}(\eta_{30} + \eta_{12})(\eta_{21} + \eta_{03})$
$\phi_7 = (3\eta_{21} - \eta_{03})(\eta_{30} + \eta_{12})\lfloor(\eta_{30} + \eta_{12})^2 - 3(\eta_{21} + \eta_{03})^2\rfloor - (\eta_{30} - 3\eta_{12})(\eta_{21} + \eta_{03})\lfloor 3(\eta_{30} + \eta_{12})^2 - (\eta_{21} + \eta_{03})^2\rfloor$
$\mu_{00} = M$ (Mass)
$\mu_{10} = 0$
$\mu_{01} = 0$
$\mu_{20} = \sum_{j=1}^{n}\sum_{i=1}^{n} f(x_i, y_j)(x_i^2 + \frac{1}{12})$
$\mu_{02} = \sum_{j=1}^{n}\sum_{i=1}^{n} f(x_i, y_j)(y_j^2 + \frac{1}{12})$
$\mu_{03} = \sum_{j=1}^{n}\sum_{i=1}^{n} f(x_i, y_j)(y_j^3)$

The behaviour of the model during the recognition of color images has been studied both in the presence and absence of noise or perturbations.

6. Structure of MicroARTMAP based pattern recognizer

The overall structure of the pattern recognizer consists of an image processor, a feature extractor, MicroARTMAP training and MicroARTMAP inference. The images (patterns) whether monochrome or color are input through the image processor. In this work, the images are engraved on a grid size of 25×25 or 40×40. Also images may have their colors chosen from a fixed palette. Here, the colors are white, black, green and yellow. However, any number of colors could be used to define the palette. The image processor receives the images that are to be trained (training patterns) or inferred by MicroARTMAP (inference patterns).

The feature extractor obtains the RST invariant features for each image, whether for training or inference. From the images submitted for training or inference, the seven moments based invariant functions, $\phi_1, \ldots, \phi_7$ are extracted by the feature extractor for presentation to MicroARTMAP. Thus, the MicroARTMAP works only on the feature vectors of the images and not on whole images. The MicroARTMAP activator functions have two modules: the training module and the inference module. The feature vectors of the training patterns and the categories to which they belong (image category) are presented to MicroARTMAP's TRAINING MODULE. The only user selectable parameter for training session is the vigilance parameter $\rho(0 < \rho < 1)$. Once the training is complete, the top–down weight vectors represent the patterns leaned. Next, the feature vectors of the images that are to be recognized/classified are presented to the inference module. MicroARTMAP now begins its classification of images by associating the feature vectors with the top down weight vectors. The category of the image is output by MicroARTMAP.

7. Examples

7.1. Recognition of alphabets and words by MicroARTMAP

Optical character recognition of hand written or printed characters is wide-spread nowadays. Images of pages in text are converted to ASCII character files for editing and combining with other files. Generally, these systems operate on typed fonts. The problem of recognition becomes more difficult for hand written alphanumeric characters. There are similarities between certain characters. A "2" may appear to be "z" or vice versa. An "a" may appear to be "q", or a "h" may appear as "n". If the recognition features are invariant under rotation, then a "d" and "p" will have the same features. Hence, some features which are not rotation invariant would distinguish these characters. Each character is thus treated as a texture and the texture features are extracted. Hu's moment invariants are used to arrive at these features of the texture. Those patterns that are similar are classified as belonging to the same class. The images that are perturbed (rotated, scaled or translated) versions of the given nominal patterns are all classified as belonging to a class. The feature extractor extracts these features from the patterns before presenting them as "pre-processed" inputs to MicroARTMAP. Weights are initialized to 1 before training. The inputs are normalized by complement coding. The number of samples is $40 \times 10 = 400$ (26 English alphabets + 4 Tamil alphabets + 10 numbers). Each input of hand written alphabet is presented in 40×40 grid size and the moment based feature extractor extracts seven features. Out of these seven features, first six are used to the MicroARTMAP since the seventh feature is negligibly small. For example B has six features as

$$B = [0.47844\ 0.16473\ 0.05568\ 0.14866\ 0.0188\ 0.06017;$$
$$- - - - - - - - - - - - - - - - - - -$$
$$- - - - - - - - - - - - - - - - - - -$$
$$0.4761\ 0.10269\ 0.055137\ 0.14588\ 0.018239\ 0.05873];$$

Number of training pairs used for each alphabet is 6 (with noise) and the recognition is 100%. Training with correct data takes 30 steps as shown in Table 2. Without considering moment invariant features, MicroARTMAP has also been tested to recognize hand written words. Each hand written alphabets (20 English alphabet + 4 Tamil alphabets) is given 7×5 matrix forms as input and the input has space of 30 patterns in total. There are 10 numbers of data for each pattern and the total number of samples is 300. After training the network, any alphabet or word is given as input and is easily recognized by the network. Table 2 gives the details of the recognition of alphabets by MicroARTMAP. Total time for training and recognition of word (WORD) is 0.5313 s.

7.2. Is classification of soil [15]

The two objectives of soil exploration and classification are to find the suitability of the soil for the construction of different structures like dams, embankments sub grade and wearing surfaces, and secondly, the effect on the fertility of soil when it is irrigated. Soils seldom exist in nature

Table 2
Alphabets recognition

Input alphabet	Output	Training step	Recognition
W (exact pattern)	10111	23rd	Correct
O (noisy pattern)	01111	15th	Correct
R (noisy)	00100	4th	Correct
D (noisy)	00100	4th	Correct
A (exact)	00001	23rd	Correct
O (noisy)	01111	15th	Correct
R (noisy)	00100	24th	Correct
Pa (noisy)	11101	14th	Correct

separately as sand, gravel or any other single component, but are usually found as a mixture with varying proportions of particles of different sizes. When soil consists of various constituents in different proportions, the mixture is given the name of the constituent that appears to have a significant influence on its behaviour. Thus, sandy clay has most of the properties of clay, but contains a significant amount of sand. The behaviour of soil mass under load depends upon many factors: the properties of the various constituents present in the mass, the degree of density saturation and the environmental conditions. There are many classification systems of soils, from among which we consider the unified soil classification system. In practice, soil classification is determined by comparing data with the existing experimental results. Hence, MicroARTMAP is applied to this problem, because existing techniques are not accurate or satisfactory.

The Bureau of Indian Standards (BIS) classifies the soil based on properties such as color of soil, percentage of gravel, percentage of sand, percentage of fine-grained particles, liquid limit and plastic limit. For input to the network, the following rule is used for the color of the soil; 0.1 – brown; 0.2 – brownish grey; 0.3 – grayish brown; 0.5 – reddish yellow; 0.7 – yellowish red. The classification of the soil is given as 0.1 – clayey soil; 0.2 – clay with medium compressibility; 0.3 – clay of low compressibility; 0.6 – silt with medium compressibility. Table 3 shows the normalized data to the MicroARTMAP. It is possible to classify the soil using MicroARTMAP.

In order to compare the efficiency of MicroARTMAP, the sequential learning neural networks (SLNN) [15] was used with the architecture (7 inputs − 6 input neurons + 1 bias), 1 hidden neuron and 1 output neuron with learning rate of 0.5 and a momentum factor of 0.0000001. It required 10,000 iterations for training. First ten samples are used for training and next eight samples are used for testing. From the weights determined in SLNN, the soil classification is given by the equation as

$$s.c. = 210.232/(1 + e^{-p}) \tag{26a}$$

where

$$p = (-0.164I_1 - 2.121I_2 - 3.521I_3 - 0.715I_4 - 10.95I_5 + 8.0619I_6 - 3.237) \tag{26b}$$

It is not possible to write the equation for soil classification by a MicroARTMAP but only classification can be done.

7.3. Plastification of clamped isotropic plate

For many generations, engineers have based the analysis and design of structures on a linear theory of elasticity assuming the material to be isotropic. But, it is common that the elastic analysis is unduly conservative because it fails to take advantage of the ability of many materials to carry stresses above the yield stress. The problem is pertained to the recognition of patterns for the prediction of load from yield patterns of elasto-plastic, clamped plates. Finite element displacement method for elasto-plastic analysis of bilinear strain hardening orthotropic plates and shells, assuming elastic unloading was developed by Whang [16]. The two basic approaches by Whang in elasto-plastic analysis are the initial stiffness approach and tangent stiffness approach, in conjunction with the Huber–Mises yield criterion and the Prandtl–Reuss flow rule in accordance with the strain hardening yield function.

The formation of plastic zones with respect to the loading is to be represented in the patterns. The MicroARTMAP architecture is trained with the patterns representing the plastic zones and their corresponding loading

Table 3
IS classification of soil

Color soil	%Gravel/18	%Sand/82	%Grain particles/84	Liquid limit/50	Plastic limit/34	IS classification	
						Actual	Micart
Soil							
0.1	0.000	0.975	0.238	0.61	0.647	0.1	0.1
0.2	0.111	0.682	0.5	0.508	0.529	0.1	0.1
0.1	0.000	0.341	0.857	0.728	0.764	0.2	0.2
0.1	0.000	0.329	0.869	0.711	0.735	0.2	0.2
0.2	0.000	0.524	0.678	0.576	0.676	0.3	0.3
0.2	0.000	0.512	0.690	0.576	0.647	0.3	0.3
0.2	0.000	0.548	0.654	0.593	0.676	0.3	0.3
0.2	0.166	0.67	0.5	0.525	0.558	0.1	0.1
0.2	0.000	0.585	0.619	0.61	0.823	0.6	0.6
0.2	0.222	0.682	0.476	0.508	0.529	0.1	0.1
0.1	0.000	0.341	0.857	0.711	0.735	0.2	0.2
0.2	0.000	0.536	0.666	0.576	0.647	0.3	0.3
0.5	0.000	0.597	0.607	0.61	0.823	0.6	0.6
0.2	0.000	0.512	0.690	0.593	0.676	0.3	0.3
0.1	0.000	0.926	0.285	0.627	0.676	0.1	0.1
0.2	0.222	0.658	0.5	0.525	0.529	0.1	0.1
0.1	0.000	0.951	0.261	0.61	0.676	0.1	0.1
0.1	0.000	0.341	0.857	0.728	0.735	0.2	0.2

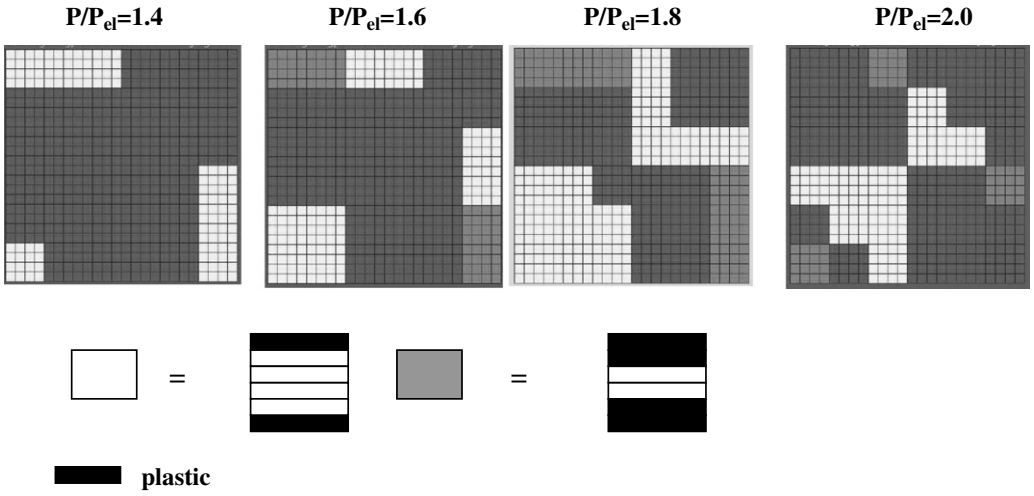

Fig. 3. Isotropic plate (clamped).

and tested for its inference capability. The uniformly loaded isotropic plates with clamped edges are assumed to have the thickness as $t = 1.0$, the Young's modulus and the Poisson's ratio as $E = 300{,}000$ kN/sq m and 0.3 and σ_0 is the yield stress = 30 kN/sq m, $E_p = 300$ kN/sq m.

Considering the doubly symmetric nature of the patterns, only a quarter of the image is presented to MicroARTMAP for training as shown in Fig. 3. A slight disturbance is made in the original patterns and these patterns are used for inference out of the training. Moment invariants are calculated for all the patterns used as data for training the architecture and are tabulated in Table 4. It is seen that MicroARTMAP is able to recognize patterns if they are slightly disturbed and it is not possible to identify patterns if the noise is too high.

The network can handle both symmetric and asymmetric patterns. However, in the case of symmetric patterns it is essential that only distinct portions of the images be trained. This is because in the case of doubly symmetric patterns, their RST invariant feature vectors $\phi_2, \ldots, \phi_7$ acquire values that are very close to 0, and ϕ_1 tends to 1. This consequently results in feature vectors which are similar, leading to misclassification of patterns.

Table 4
Moment invariants for yield pattern for clamped isotropic plate

*M*1	*M*2	*M*3	*M*4	*M*5	*P*/*P*(*y*)
0.93	0.26	0.321	0.938	0.483	1.4
0.568	0.0874	0.041	0.205	0.016	1.6
0.275	0.627	0.004	0.018	0.0001	1.8
0.228	0.015	0.00395	0.0137	0	2.0
0.935	0.267	0.321	0.938	0.483	1.4
0.596	0.0904	0.041	0.205	0.016	1.6
0.258	0.0217	0.004	0.018	0.0001	1.8
0.228	0.015	0.00375	0.0137	0	2.0
0.938	0.268	0.321	0.938	0.483	1.4
0.586	0.0674	0.041	0.205	0.016	1.6
0.285	0.047	0.0048	0.018	0.0001	1.8
0.228	0.015	0.00395	0.0137	0	2.0
0.939	0.269	0.321	0.938	0.483	1.4
0.576	0.0784	0.041	0.205	0.0116	1.6
0.275	0.0217	0.0214	0.067	0.0031	0.8
0.228	0.015	0.00395	0.0137	0	2.0
0.937	0.269	0.321	0.938	0.483	1.4
0.568	0.0874	0.041	0.205	0.016	1.6

7.4. Prediction earthquake parameters from response spectra

In the last century, India and other countries have had a number of the world's greatest earthquakes. More than 60% of the area in India is considered prone to damaging earthquakes. The north-eastern region of the country as well as entire Himalayan belt is susceptible to great earthquakes of magnitude more than 8. Besides these, even the peninsular India is prone to damaging earthquakes. The January 26, 2001, Earthquake at Bhuj, Gujarat has been the most damaging earthquake in the last five decades. The M7.9 quake has caused a huge loss of life and property. Housing and safety are the basic human needs. Structures adequately designed for usual loads need not necessarily be safe for earthquake forces. In case of design to earthquake loading, it is not practical and economically viable to design the structures to remain within elastic limits. Cracking of concrete and yielding of steel, which would be considered unacceptable for usual types of loading are depended on to dissipate the seismic energy without collapse for ground shaking that may take place infrequently. It is also necessary to generate artificial accelerograms and study the behaviour of structures due to various types of earthquakes simulated.

Proper ground motions are required to assess the seismic response of a structure. It is necessary to generate artificial earthquake ground motions at a site because recorded accelerograms are generally very limited. Trifunac and Brady [17] defined the significant duration as a function of the magnitude (M) and epi-central distance (R). Also Trifunac and Lee [18] developed as empirical model for Fourier spectrum in terms of M, R and attenuation

Table 5
M, *S*, *H* and *R* for different response spectra

S. no.	*M* (actual)	*M* (normal)	*S* (actual)	*S* (normal)	*H* (actual)	*H* (normal)	*R* (actual)	*R* (normal)
1	6	0.166667	0	0.166667	1	0.03125	30	0.083333
2	6	0.166667	0	0.166667	1	0.03125	50	0.916667
3	6	0.166667	0	0.166667	30	0.9375	30	0.083333
4	6	0.166667	0	0.166667	30	0.9375	50	0.916667
5	6	0.166667	2	0.833333	1	0.03125	30	0.083333
6	6	0.166667	2	0.833333	1	0.03125	50	0.916667
7	6	0.166667	2	0.833333	30	0.9375	30	0.083333
8	6	0.166667	2	0.833333	30	0.9375	50	0.916667
9	8	0.833333	0	0.166667	1	0.03125	30	0.083333
10	8	0.833333	0	0.166667	1	0.03125	50	0.916667
11	8	0.833333	0	0.166667	30	0.9375	30	0.083333
12	8	0.833333	0	0.166667	30	0.9375	50	0.916667
13	8	0.833333	2	0.833333	1	0.03125	30	0.083333
14	8	0.833333	2	0.833333	1	0.03125	50	0.916667
15	8	0.833333	2	0.833333	30	0.9375	30	0.083333
16	8	0.833333	2	0.833333	30	0.9375	50	0.916667
17	6	0.166667	1	0.5	15.5	0.484375	40	0.5
18	8	0.833333	1	0.5	15.5	0.484375	40	0.5
19	7	0.5	0	0.166667	15.5	0.484375	40	0.5
20	7	0.5	2	0.833333	15.5	0.484375	40	0.5
21	7	0.5	1	0.5	1	0.03125	40	0.5
22	7	0.5	1	0.5	30	0.9375	40	0.5
23	7	0.5	1	0.5	15.5	0.484375	30	0.083333
24	7	0.5	1	0.5	15.5	0.484375	50	0.916667
25	7	0.5	1	0.5	15.5	0.484375	40	0.5
26	7.5	0.666667	0	0.166667	22	0.6875	45	0.708333
27	7.5	0.666667	1	0.5	22	0.6875	35	0.291667
28	7.5	0.666667	2	0.833333	8	0.25	45	0.708333
29	6.5	0.333333	0	0.166667	8	0.25	35	0.291667
Minimum	6	0	1	30				
Maximum	8		2		30		50	
Min (taken)	5.5		−0.5		0		28	
Max (taken)	8.5		2.5		32		52	

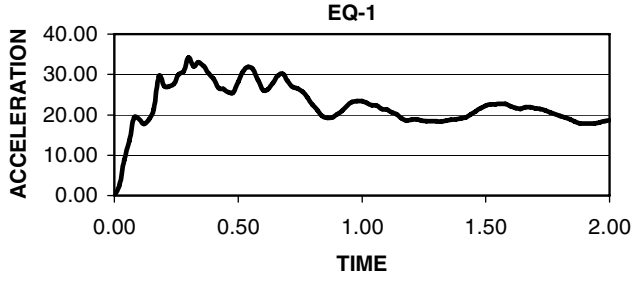

Fig. 4. Response spectra for $M = 6$, $S = 0$, $H = 1$, $R = 30$.

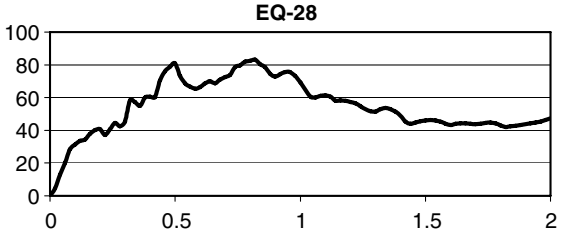

Fig. 6. Response spectra for $M = 7.5$, $S = 2$, $H = 8$, $R = 45$.

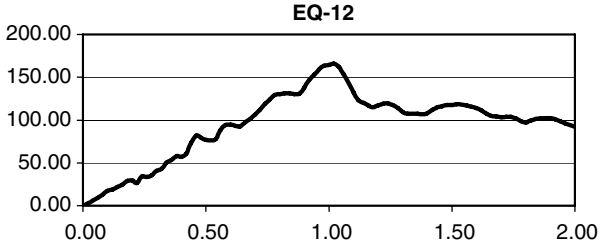

Fig. 5. Response spectra for $M = 8$, $S = 0$, $H = 30$, $R = 50$.

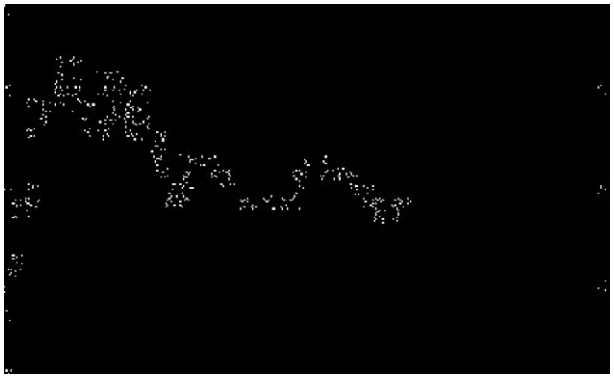

Fig. 7. Black and white figure of Fig. 3.

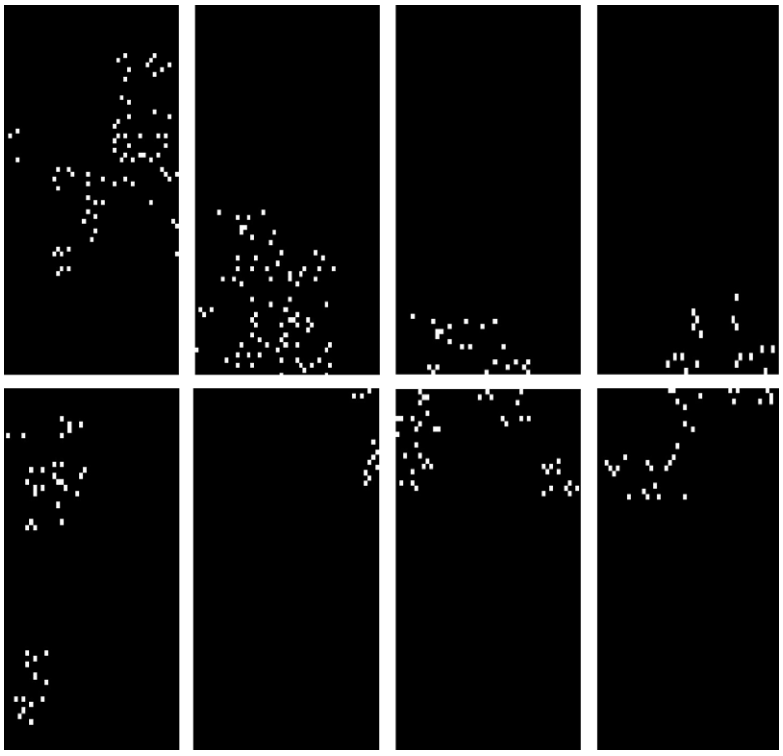

Fig. 8. The figure is divided into eight parts. Number of black counts in each part is $C1 = 4731$, $C2 = 4881$, $C3 = 4977$, $C4 = 4982$, $C5 = 4732$, $C6 = 4882$, $C7 = 4978$, $C8 = 4983$.

Table 6
Black pixel count in the split response spectra

$C1$	$C2$	$C3$	$C4$	$C5$	$C6$	$C7$	$C8$
0.6871	0.7419	0.9080	0.9365	0.6886	0.7435	0.9100	0.9385
0.4214	0.7452	0.7420	0.7827	0.4229	0.7468	0.7440	0.7846
0.8214	0.7613	0.8540	0.8038	0.8229	0.7629	0.8560	0.8058
0.5286	0.7694	0.8200	0.8481	0.5300	0.7710	0.8220	0.8500
0.7114	0.7839	0.9640	0.9615	0.7129	0.7855	0.9660	0.9635
0.3100	0.9274	0.8640	0.8538	0.3114	0.9290	0.8660	0.8558
0.4871	0.7597	0.7520	0.8692	0.4886	0.7613	0.7540	0.8712
0.1243	0.7403	0.7680	0.7462	0.1257	0.7419	0.7700	0.7481
0.6357	0.6000	0.4800	0.6077	0.6371	0.6016	0.4820	0.6096
0.4529	0.9677	0.9700	0.7673	0.4543	0.9694	0.9720	0.7692
0.8386	0.8065	0.6300	0.5712	0.8400	0.8081	0.6320	0.5731
0.9971	0.9677	0.9620	0.7038	0.9986	0.9694	0.9640	0.7058
0.9786	0.8645	0.8760	0.9385	0.9800	0.8661	0.8780	0.9404
0.8443	0.7194	0.5880	0.6212	0.8457	0.7210	0.5900	0.6231
0.7214	0.7661	0.6160	0.5577	0.7229	0.7677	0.6180	0.5596
0.6500	0.5387	0.4620	0.5135	0.6514	0.5403	0.4640	0.5154
0.5500	0.5371	0.5740	0.6346	0.5514	0.5387	0.5760	0.6365
0.5157	0.7258	0.6120	0.5423	0.5171	0.7274	0.6140	0.5442
0.5414	0.7258	0.5380	0.5096	0.5429	0.7274	0.5400	0.5115
0.8243	0.6855	0.6740	0.6442	0.8257	0.6871	0.6760	0.6462
0.4557	0.8065	0.6600	0.6808	0.4571	0.8081	0.6620	0.6827
0.7257	0.6226	0.5480	0.6038	0.7271	0.6242	0.5500	0.6058
0.8500	0.6097	0.5860	0.7635	0.8514	0.6113	0.5880	0.7654
0.7186	0.7435	0.6040	0.6096	0.7200	0.7452	0.6060	0.6115
0.1186	0.4758	0.3240	0.2096	0.1200	0.4774	0.3260	0.2115
0.8600	0.9677	0.8660	0.8058	0.8614	0.9694	0.8680	0.8077
0.9943	0.8048	0.7800	0.7904	0.9957	0.8065	0.7820	0.7923
0.4271	0.1435	0.0360	0.1538	0.4286	0.1452	0.0380	0.1558
0.2629	0.5645	0.3720	0.3365	0.2643	0.5661	0.3740	0.3385

function related to a site condition (S) and focal depth (H). Hence, initial information is defined in terms of M, R, S, H. Lee and Han [19] have developed efficient neural network based models for the generation of artificial earthquake

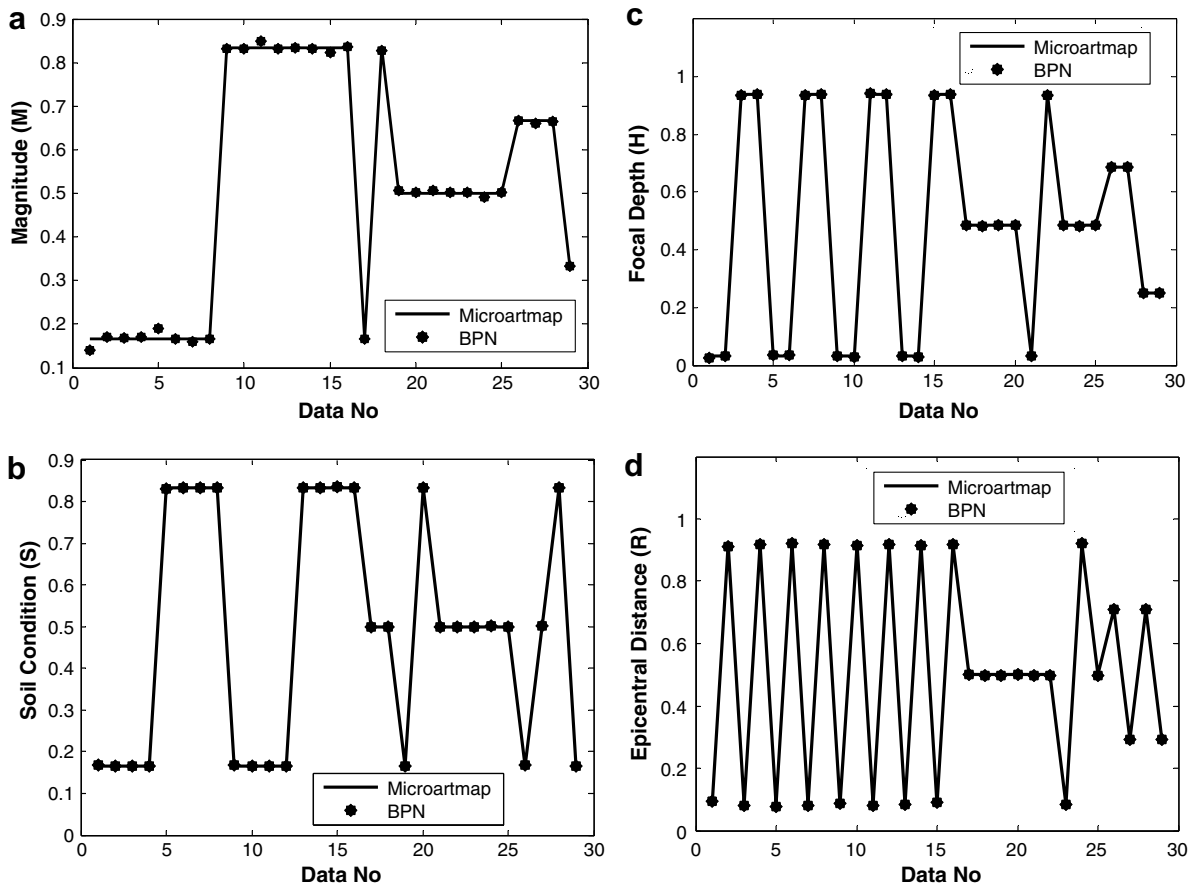

Fig. 9. Comparison of MIRCRO ARTMAP with BPN.

and response spectra. Several examples were given to verify the developed models.

Rajasekaran et al. [20] developed wavelet and principal component analysis for the generation of artificial earthquake motion records using initial parameters M, S, H and R. Most of the seismic design procedures have presented the well defined design spectrum rather than the time history. Hence, it is important to generate the accelerogram compatible with a target spectrum which can be called inverse problem.

In this paper, the problem is pertained to solving the inverse problem for the prediction of Magnitude, Site condition, Focal depth and Epi-central distance from response spectrum [21]. The actual and normalized values of M, R, S and H are given in Table 5. Three different spectra are given in Figs. 4–6 for different earthquakes 1, 12 and 28 of Table 5. Any given response spectrum is changed to black and white figure and it is divided in to eight-parts using a program developed in **MATLAB** and the number of black pixels in all the eight parts are counted and are denoted by $C1$, $C2$, …, $C8$ (see Figs. 7 and 8). These counts in normalized form are given as inputs for all the 29 data as shown in Table 6 and corresponding Magnitude, Site condition, Focal depth and epi-central distance are given as four outputs to MicroARTMAP. Training is successfully carried out for 29 different patterns. The range of the training patterns is limited to 6.0–8.0 for M. 30–50(m) for R. 0, 1, 2 for S (classification by UBC) and 1–30(m) for H. In this problem, the learning rate, vigilance parameter on output and step size is assumed as 1, 0.9 and 0.02, respectively.

A slight disturbance is made in the original patterns and these patterns are used for inference out of the training. It is seen that MicroARTMAP is able to recognize patterns if they are slightly disturbed and it is not possible to identify patterns if the noise is too high. It is possible to classify the Magnitude, Site condition, Focal depth and epi-central distance of any given response spectrum using MicroARTMAP.

When the same problem is presented to BPN (available in tool box of MATLAB), it requires 2800 epochs for convergence. Fig. 9 shows the comparison of M, S, H and R obtained by MicroARTMAP and BPN. MicroARTMAP does not take much time for training as BPN does.

8. Conclusions

In this paper, the pattern recognition capability of MicroARTMAP has been discussed. The architecture augmented with a moment based feature extractor exhibits an excellent capability to recognize patterns by working on the

RST invariant feature vectors of the patterns rather than the patterns themselves. The augmented architecture can handle both symmetric and asymmetric patterns. In the case of asymmetric patterns, the RST invariant functions turn out to be the same for all perturbations of a given pattern. Hence, MicroARTMAP has no difficulty in recognizing perturbed patterns since it only calls for associating the same feature vectors with top–down weights vectors. This results in the invocation of the same category node with correct identification of the perturbed pattern. However, in the case of symmetric patterns it is essential that only distinct portions of the images be trained. In the case of multi-symmetric patterns, it is sufficient to consider $1/2n$ of the portion of the image.

It is seen from the first example, MicroARTMAP recognizes hand written characters (English and Tamil) and words. When the MicroARTMAP is augmented with moment based feature extractor, it can recognize hand written alphabets and numerals. Time taken for soil classification is much less compared to other architectures such as SLNN.

The prediction of load from yield pattern by using MicroARTMAP is done quite accurately. It is also seen that inverse problem could be handled by MicroARTMAP such as prediction of earthquake parameters from response spectra. Again comparing with other neural network architecture such as BPN, the time taken by MicroARTMAP is less.

Moreover, the potential of the proposed MicroARTMAP as a tool for pattern recognition problems has been illustrated in the examples presented.

Acknowledgements

The authors thank Prof. Eduardo Gomez-Sanchez for his suggestions and help. The authors also thank the management of PSG College of Technology and Dr. R. Rudramoorhty, Principal, for providing necessary facilities for the completion of the work reported in this paper. The authors also thank the anonymous reviewers for their suggestions in improving the standard of the manuscript.

References

[1] Chao CJ, Cheng FP. Fuzzy pattern recognition model for diagnosing cracks in RC structures. J Comp Civil Eng, ASCE 1998;12(2):111–9.
[2] Ishizuka M, Fu KS, Yao JTP. A rule based inference with fuzzy set for structural damage assessment. In: Gupta MM, Sanchez E, editors. Approximate reasoning in decision process. North Holland: Amsterdam; 1982. p. 261–75.
[3] Watada J, Fu KS and Yao JTP. Linguistic assessment of structural damage, Rep CE-STR-84-30, Purdue University, West Lafayette, Ind.; 1984.
[4] Kosko B. Neural networks and fuzzy systems: a dynamical systems approach to machine intelligence. Englewood Cliffs (NJ): Prentice-Hall; 1992.
[5] Yamakawa T, Tomoda S. A fuzzy neuron and its application to pattern recognition. In: Proceedings of the third international fuzzy system association congress; 1989. p. 30–8.
[6] Moore B. ARTI and pattern clustering. In: Touretzky D, Hinton G, Sejnowski T, editors. Proceedings of 1988 connectionist models, Summer School. Morgan Kaufmann Publishers; 1998. p. 174–85.
[7] Carpenter GA, Gjaja M. Fuzzy ART choice functions, Technical Report AS/CNS-TR 93-060. In: Proceedings of the world congress on neural networks (WC NN'94), Boston University; 1993.
[8] Carpenter GA, Grossberg S, Markuzon N, Reynolds JH, Rosen DB. Fuzzy Adaptive Resonance Theory – a neural network architecture for incremental supervised learning of analog multidimensional maps. IEEE Trans Neural Networks 1998;3(5):698–712.
[9] Kasuba T. Simplified fuzzy ARTMAP 1993:18–25, Nov.
[10] Sanchez EG, Dimitriadis YA, Izquierdo JMC, Coronado JL. μARTMAP: use of mutual information for category reduction in fuzzy ARTMAP. IEEE Tran Neural Networks 2002;13(1).
[11] Rajasekaran S, Vijayalakshmi Pai GA. Image recognition using simplified Fuzzy Art Map augmented with a moment based feature extractor. Pattern Recogn, Artif Intell 2000;14(8):1081–94.
[12] Rajasekaran S, Vijayalakshmi Pai GA. Simplified fuzzy ARTMAP as pattern recognizer. J Comput Civil Eng 2000;14(2):92–9.
[13] Rajasekaran S, Amal Raj R. Image recognition using analog – ART1 Architecture augmented with moment-based feature extractor. Neuro Computing 2004;56:61–77.
[14] Rosenblatt F. Principles of neuro dynamics. Spartan Books; 1961.
[15] Rajasekaran S, Deepa Suresh, Vijayalakshmi Pai GA. Application of sequential learning neural networks to civil engineering problems. Eng Comp 2002;18:138–47.
[16] Whang B. Elasto plastic orthotropic plates and shells. In: Proceedings of the symposium on application of finite element methods in civil engineering, ASCE; November 1969. p. 481–515.
[17] Trifunac MD, Brady AG. A study of strong earthquake ground motion. Bull. Seismol. Soc. Am. 1975;45(3):581–626.
[18] Trifunac MD, Lee VW. Empirical models for scaling Fourier amplitude spectra of strong ground accelerations in terms of Earthquake magnitude, source to station distance, site intensity and recording site condition. Soil Dyn Earthq Eng 1989;8(3):110–25.
[19] Lee SC, Han SW. Neural – network based models for generating artificial earthquakes in response spectra. Comp Struct 2002;80: 1627–38.
[20] Rajasekaran S, Vasuki Latha, Lee SC. Generation of artificial earthquake records using wavelets and principal component analysis. J Earthq Eng 2006;10(5):665–82.
[21] Vasuki Latha, AR. Generation of earthquake and response spectra using neural networks combined with wavelet transforms and principal component analysis. ME thesis submitted to Anna University, May, Coimbatore, India; 2004.